Parametric Study of Probe Positioning Errors in Articulated Spherical Near-field Test Systems for mm-Wave Applications

Daniël Janse van Rensburg, Stuart F. Gregson
Nearfield Systems Inc.
19730 Magellan Drive
Torrance, CA, 90502, USA
drensburg@nearfield.com, sgregson@nearfield.com

***Abstract* — This paper describes an articulated arm spherical near-field scanner design which transports a probe over a hyper-hemispherical surface that surrounds a stationary test antenna. Surface profile data collected with a laser tracker is presented and a parametric study performed to investigate the viability of testing at mm-wave frequencies is described. Parameters such as probe radial distance, and angular positioning are investigated to assess to what extent spherical near-field testing can be performed using this structure.**

I. Introduction

In recent years, planar near-field antenna testing at mm-wave and sub-mm-wave frequencies have become commonplace [1, 2, 3] with many of the RF and mechanical challenges being successfully identified and addressed [4, 5, 6]. As the number and variety of test applications at these higher frequencies have increased, so too has the need for additional antenna test systems that are not necessarily limited to characterizing high gain antennas. Spherical near-field test systems address this need perfectly with new high precision spherical near-field systems being implemented in recent years that satisfy the stringent alignment requirements imposed by the spherical geometry [7]. Most conventional spherical near-field positioning systems require the antenna to rotate about one- or two-axes. This paper will describe a novel articulated design which transports a probe over a hyper-hemispherical surface in front of an inertial antenna which is crucial in cases where motion of the antenna is undesirable, due to its sensitivity to gravitational deformation, delicacy of the feeding mechanism, *etc*. [8, 9]. This paper describes a parametric study that was undertaken to investigate the viability of testing at mm-wave frequencies using positioners implementing an articulated θ/ϕ robotic positioning sub-system. Parameters such as probe radial distance, and angular positioning were investigated to assess to what extent spherical near-field testing could be performed using commercially available positioners.

II. Articulated Spherical Near-Field Antenna Test System

The spherical near-field (SNF) antenna test system of interest here is as illustrated in Figure 1. This consists of a 500 mm positioner mounted on a large floor stand. This positioner defines the horizontal ϕ-axis of rotation and this coincides with the *z*-axis of the measurement coordinate system. A second rotary stage is attached to this stage at an angle of 90° to the ϕ-axis and this second stage forms the θ-axis of a conventional right handed polar spherical coordinate system. A third rotary stage is attached to the θ-stage at an angle of 90° to the θ-axis and this third stage forms the χ-axis. The combined motion of the ϕ and θ stages allows the probe tip to describe the trajectories located on a spherical surface centred about the intersection of those orthogonal axes and whose definition is in accordance with standard spherical near-field (SNF) theory. Crucially, and as is the case for planar measurements, data is acquired across a two-dimensional sampling interval with the antenna under test (AUT) remaining entirely at rest (a feature of particular interest when measuring on-chip antennas).

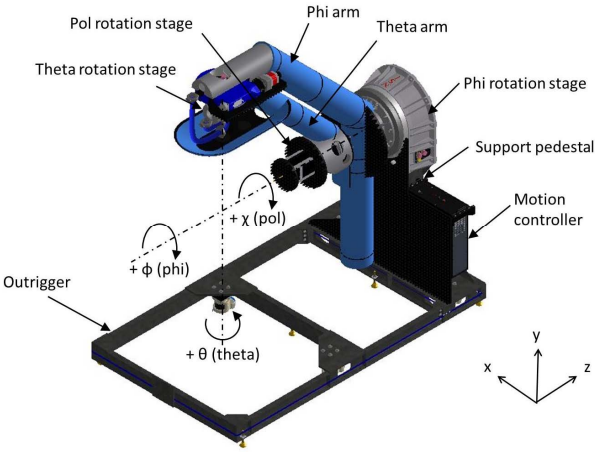

Fig. 1. Schematic representation of the NSI-700S-86 articulated spherical near-field antenna test system showing the attendent spherical measurement coordinate system.

Figure 2 contains a picture of the partially absorber covered system undergoing factory testing. The stationary AUT can be seen to the right of the image and comprises a yellow pyramidal horn. Here, the AUT is nominally installed centered about the intersection of the θ- and ϕ-axes of the spherical robotic positioners with the horizontal boresight direction coincident and synonymous with the pole of the spherical measurement coordinate system.

Fig. 2. Spherical near-field system undergoing factory testing. The stationary AUT can be seen positioned over the centre of rotation in a polar mode allowing near 4π steradian coverage with negligible blockage.

The NSI-700S-86 system is sufficiently large to incorporate mm-wave frequency up and down converter modules as part of the probe carriage assembly whilst maintaining a probe tip radius of approximately 0.5 m, with the exact value depending upon the dimensions of the mm-wave module and probe. The mm-wave modules are exchanged to cover the relevant waveguide frequency bands, leaving the RF equipment rack and cabling portion of the RF sub-system intact, making for a convenient modular and upgradable test system. All positioners contain integrated RF rotary joints to maximize the phase stability of the guided wave path during testing with the ϕ-axis positioner also containing a slip-ring assembly for passing power and control lines to successive positioners.

Of particular interest here is the deformation of the structure under the influence of the local gravity vector as this deformation introduces a positional error, and when not corrected, corresponds to an uncertainty in the measurement. Figure 2 and Figure 3 below show typical structural deformations obtained from a mechanical Finite Element Analysis (FEA) of the structure. Here, the defection shown has been grossly exaggerated for the purposes of illustration.

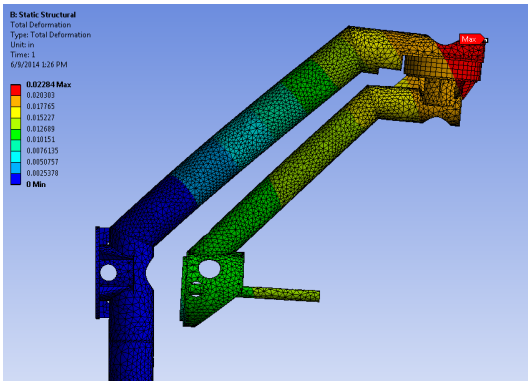

Fig. 3. Finite element analysis of articulated spherical near-field robotic positioning sub-system, θ = 0° and ϕ = 0° position shown.

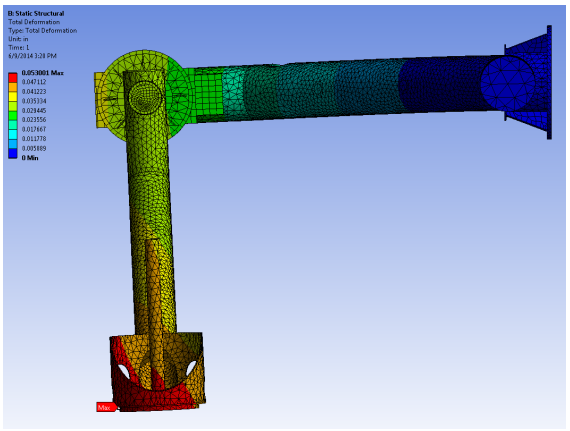

Fig 4: Finite element analysis of articulated spherical near-field robotic positioning sub-system, θ = 90°, ϕ = -90° shown.

Actual data, similar to the predicted FEA results, can be obtained from laser tracker dimensional measurements. These results allow us to establish a perturbed (θ′, ϕ′, *r*′) grid, based on a regular (θ, ϕ, *r*) SNF grid. Results obtained for *r*′ as a function of (θ, ϕ) are depicted below in Figure 5 in the form of a false colour checkerboard plot.

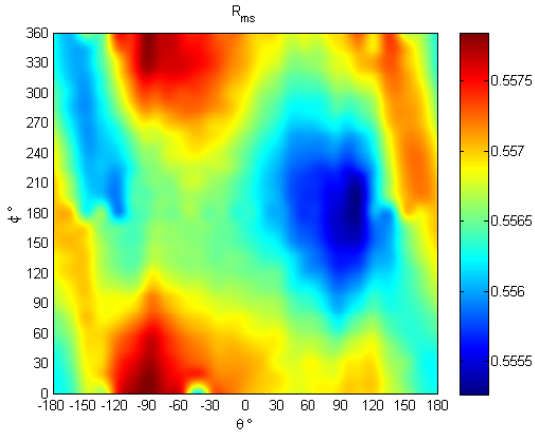

Fig 5. Scanner radius *r*′ shown as a function of (θ, ϕ). The radius variation observed is from 555.5 mm to 557.5 mm.

This result shows that the actual measurement radius *r*′ deviates from an ideal constant by approximately ±1 mm across the redundant 4π steradian spherical sampling surface. Although not shown, similar error distributions were obtained for θ′ and ϕ′ (deviations from ideal of ±0.15° were measured for some orientations) and this grid allows for evaluation of the impact of structure deformation on the derived radiation pattern data.

III. Results of CEM Simulation

Using the laser tracker measured results presented in Section II above a computational electromagnetic (CEM) simulation was performed to assess the impact of the mechanical deformations on the electromagnetic measurements. Three simulated sources were considered (as a consequence of the need for brevity, results for only two cases are presented herein), the first a half wavelength dipole

radiating at 75 GHz. The second and third sources comprised a 6 mm by 6 mm square aperture radiating at 75 GHz, one facing the sphere pole and other facing the equator. In all instances the probe radial distance was set to 556.7 mm to correspond with the scanner ideal radial dimension. In the case of the second and third sources, each was also offset by an 80 mm linear distance so as to increase the required sampling density in order to assess the sensitivity to angular sampling uncertainty. Prior studies have shown that absolute angular uncertainty is not as significant as angular uncertainty as a fraction of the angular sampling interval [7]. These simulated source distributions were selected to represent two high gain cases at a typical operational frequency, and a low gain case. The test scenarios are summarized and compared within Table I below.

TABLE I. SUMMARY OF CEM TEST CASES.

Case#	Size [mm]	Freq [GHz]	λ [mm]	Offset [mm]	Array Plane	Sample spacing [Deg]	Probe distance [λ]
1	2	75	4	0	n/a	5	139
2.1	6 x 6	75	4	0	x-z	5	139
2.2				80	x-z	1	
3.1	6 x6	75	4	0	x-y	5	139
3.2				80	x-y	1	

For source #1 a SNF sampling density of 5° was selected although a much reduced density would have sufficed. The primary purpose of this simulation was to assess the impact of the radial variation of the scanner on resulting far-field antenna pattern data. The source in this case was a simple electric dipole located coaxial to the scanner *z*-axis and this was initially used to compute a reference far-field pattern. By introducing the measured probe positional errors, it was possible to obtain a second pattern which then allows the impact of the scanner deformation for this particular case to be assessed. The radial variation was determined from laser tracker measurements and was found to be approximately ±1 mm, which translated to ±90° of phase change (ΔΦ) at the simulation frequency as $\Delta\Phi = 2\pi/\lambda\Delta r$ where λ is the free space wavelength, and Δr is the maximum radial variation. Thus, one would expect the impact of this error to be significant. Figure 6 below confirms this supposition since from observation an error to signal level due to this variation of *circa* -12 dB is evident (top). By applying a phase compensation function to the simulated/measured near-field data that is equal to the measured radial distance variation, it is possible to apply a first order correction and hence compensate for this effect. This was confirmed by a correction in the simulated/measurement and a reduction in the effective noise floor to < -50 dB was achieved (bottom).

For source #2.1 (as defined within Table I above) typical far-field pattern data at 75 GHz is shown below in Figure 7. The source in this instance is located in the *x*-*z* plane (corresponding to an equatorial acquisition mode) and therefore radiates towards the ceiling of the chamber so as to emulate the on-chip antenna measurement case that is most likely to be encountered in practice. For this source a SNF sampling density of 5° was also selected for convenience. A reference and perturbed pattern was again compared to assess the impact of the probe positional errors as measured using the laser tracker. Figure 8 below shows the reference pattern, *i.e.* the pattern obtained without radial distance correction together with the case with the correction having been applied. Again, the corrected case is indistinguishable from the reference pattern, further highlighting the fact that the radial distance variation is the dominant component within the uncertainty budget and that again small variations in spherical angles θ and ϕ do not have a significant impact in this instance.

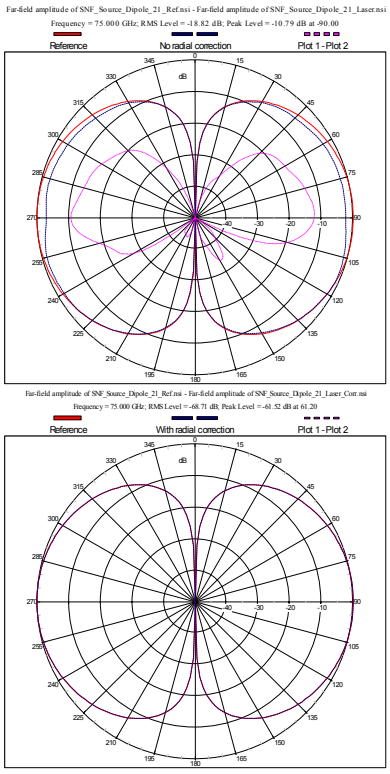

Fig 6. Source #1 (dipole on z-axis) as measured without radial distance correction. Reference is shown as solid line.

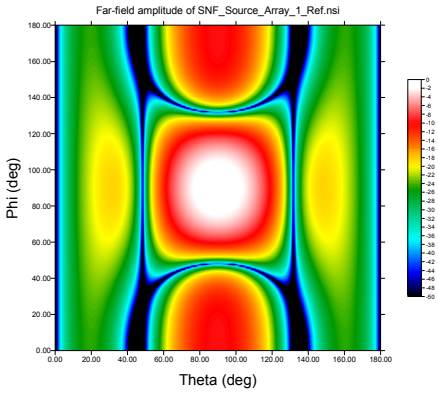

Fig 7: Source #2.1 (6 mm x 6 mm aperture) reference near-field amplitude data set at 75 GHz.

If source #2.1 is offset from the coordinate system origin by 80 mm (denoted as source #2.2) a higher sampling density is required for making valid SNF acquisitions and the angular sampling interval is reduced to 1°. If the same positional errors are introduced, the data depicted in Figure 9 are obtained. Here, the corrected case is again almost indistinguishable from

the reference pattern, except for some minor differences observed at 160° - 180°. The results again emphasize that the radial distance variation of ±90° is the dominant component within the uncertainty budget and that angular variations of up to ±0.15° in θ and ϕ are of only secondary importance. It should be noted that in the case of source 2.1 the angular uncertainty of the system is roughly 5°/±0.15° = 33 times smaller than the sampling interval. In the case of source 2.2 the angular uncertainty of the system is roughly 1°/±0.15° = 7 times smaller than the sampling interval and the effect starts to be noticed in the resulting far-field radiation patterns.

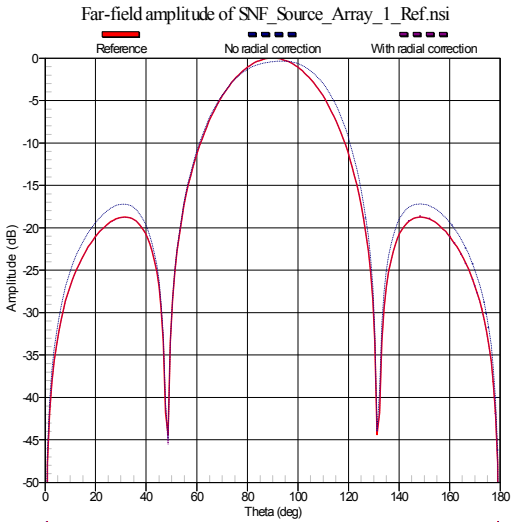

Fig 8. Radiation patterns extracted for source #2.1. Solid line depicts reference and perturbed pattern after correction of radial variation. Dashed line depicts case without radial distance correction.

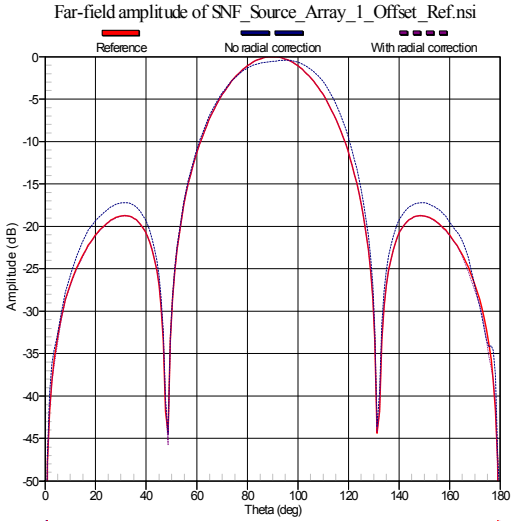

Fig 9. Radiation patterns extracted for source #2.2. Solid line depicts reference and perturbed pattern after correction of radial variation. Dashed line depicts case without radial distance correction.

IV. Summary And Conclusions

The data presented above represents the preliminary results of a parametric study to assess the suitability of an articulated arm SNF scanner for mm-wave antenna testing. A mechanical finite element analysis was initially used to characterize and design the positioning system with laser tracker dimensional measurements being obtained to characterize the system in terms of structural deflection after construction. This gravitationally induced structural deformation affects radial distance and angular positioning. This data was subsequently used to generate simulated/measured data sets for three different types of radiators in order to determine the impact of the structural deflection on spherical near-field measurements.

The results presented above show a high sensitivity to probe radial distance variation. This is not unexpected since the variation observed was in the order of ±1 mm (*i.e.* ±90° of phase at 75 GHz). First order correction for radial distance variation was performed by counter adjustment of the phase value of each measured tangential electric field component data point in the SNF data set and this proved to be a very successful compensation strategy, *c.f.* the "*k*-correction" technique for planar near-field testing [10]. This proved to be a viable and practical correction technique, without which this type of test system may be rendered of limited use at mm-wave frequencies. In a prior study [7] of a different type of SNF positioning system it was shown that derived far-field results were insensitive to λ/10 probe radius variations. However, for the scanner design considered here such a small radial distance variation specification would not be feasible in a compact, economical viable package.

References

[1] D. Slater, "A 550 Ghz Near-Field Antenna Measurement System for The NASA Submillimeter Wave Astronomy Satellite", Antenna Measurement Techniques Association Conference, October 3-7, 1994.

[2] D. Slater, P. Stek, R. Cofield, R. Dengler, J. Hardy, Robert Jarnot, Ray Swindlehurst, "A Large Aperture 650 GHz Near-Field Measurement System for the Earth Observing System Microwave Limb Sounder", Antenna Measurement Techniques Association Conference, 2001.

[3] P.W. Bond, G.A. Ediss, "Design, Alignment, and Calibration Requirements for a Submillimeter Wave Frequency Tiltable Lightweight Scanner", Antenna Measurement Techniques Association Conference, 2007.

[4] D. Janse van Rensburg, "A Technique To Evaluate The Impact of Flex Cable Phase Instability on mm-Wave Planar Near-Field Measurement Accuracies", ESA ESTEC

[5] D. Janse van Rensburg, "Compensation for Probe Translation Effects in Dual Polarized Planar Near-Field Antenna Measurements", Antenna Measurement Techniques Association Conference, 2008.

[6] D. Janse van Rensburg, G.E. Hindman, "An Overview of Near-Field Sub-millimeter Wave Antenna Test Applications", COMITE Conference, Czech Republic, 23-24 April, 2008.

[7] D. Janse van Rensburg, J. Wynne, "Parametric Study of Probe Positioning Errors in Spherical Near-field Test Systems for mm-Wave Applications", IEEE APS/URSI, Conference Chicago, 2012.

[8] G.E. Hindman, H. Tyler, "High Accuracy Spherical Near-Field Measurements on a Stationary Antenna", Antenna Measurement Techniques Association Conference, 2010.

[9] D. Titz, M. Kyrö, F. Ferrero, S. Ranvier, C. Luxey, P. Brachat, G. Jacquemod, and P. Vainikainen, "Measurement Setup and Associated Calibration Methodology for 3D Radiation Pattern of Probe-fed Millimeter-wave Antennas", Loughborough Ant. & Prop. Conf. 2011, Loughborough (UK), 14-16th Nov. 2011.

[10] L.E. Corey, E.B. Joy, "On Computation of Electromagnetic Fields on Planar Surfaces From Fields on Nearby Surfaces", IEEE Transactions on Antennas and Propagation, March 1981; AP-29, pp. 402.